Journal of Power Sources 195 (2010) 8177–8184

Contents lists available at ScienceDirect

Journal of Power Sources

journal homepage: www.elsevier.com/locate/jpowsour

Studies of the deformation styles of the rubber-pad forming process used for manufacturing metallic bipolar plates

Yanxiong Liu [a], Lin Hua [a,*], Jian Lan [b], Xi Wei [b]

[a] Hubei Key Laboratory of Advanced Technology of Automotive Parts, Wuhan University of Technology, Wuhan, China
[b] School of Material Science and Engineering, Wuhan University of Technology, Wuhan, China

ARTICLE INFO

Article history:
Received 24 May 2010
Accepted 21 June 2010
Available online 30 June 2010

Keywords:
Rubber pad forming
Concave and convex deformation styles
Metallic bipolar plate
Fuel cell

ABSTRACT

Rubber pad forming as a novel stamping technique has been widely used in the deep drawing, bulging, blanking, and flanging processes. It is a feasible method for manufacturing metallic bipolar plates, the surface of which has multi-array flow channels. For a single channel's fabrication, there are two different deformation styles: concave and convex. In this paper, the deformation characteristics of the two deformation styles are analyzed in detail with numerical simulation and experimental methods. The proper application conditions of the concave and convex deformation styles used to fabricate a certain metallic bipolar plate have been determined. If the ratio of the channel width to the rib width $w/s > 1$, the concave style is more appropriate; otherwise, the convex style is preferred. Based on this theory, a bipolar plate sample ($w/s < 1$) is successfully manufactured by the convex rubber-pad forming process.

1. Introduction

Rubber pad forming is a novel stamping method for shim sheet metal forming, and this method has been increasingly used in the automotive, energy, electronic and aeronautic industries [1–5]. Compared with the conventional stamping process, this method only requires manufacturing one rigid die according to the shape of the part and the other rigid die is replaced by a rubber pad. The main advantages of this forming process are that the forming equipment is simple and the quality of its products is high [6]. Because just one rigid die needs to be accurately manufactured, the time and cost can be greatly reduced, and, moreover, the rubber pad and rigid die are not required to be assembled precisely. Furthermore, this method can greatly improve the formability of the blank to be shaped because the contact surface between the rigid die and the rubber pad is flexible.

Micro/meso forming processes have recently attracted wide attention of the manufacturers and researchers, and the rubber-pad forming process is very suitable for micro-sheet forming because of the advantages just mentioned above. Peng et al. [7] investigated the micro/meso sheet soft punch stamping process with numerical simulation and experiments. They mainly focused on the effect of the metal sheet grain size on the deformation behavior as it plays an important role in determining its deformation behavior at the micro/meso scale.

Many other researchers have investigated the rubber-pad forming process. Browne and Battikha [8] described a rubber-pad forming process for manufacturing an aircraft wing or tail flap. They investigated the capability of the process and optimized the process parameters to ensure a defect-free product. Salau [9] optimized the process by using numerical simulation and experiments. Dirikolu and Akdemir [10] investigated the significant parameters associated with the rubber-pad forming process using numerical methods. Ramezani et al. [11] studied the friction behavior of the rubber-pad forming process. The research shows that the theoretical static and kinetic friction models have a better correlation with experimental results compared to the traditional Coulomb friction model. In the previously mentioned studies, attention has been concentrated on the deformation of large parts, the deformation characteristics of which differ greatly from those of micro-parts. Liu and Hua [12] studied the rubber-pad forming process to manufacture metallic bipolar plates used in proton exchange membrane fuel cells (PEMFC). On the surface of the metallic bipolar plate, there are multi-array flow channels. The rubber-pad forming process is found to be a novel and feasible method for fabricating these channels.

The metallic bipolar plate sample and the equipment used in the rubber-pad forming process to fabricate the bipolar plate are shown in Fig. 1. The three flow channels that are made in the bipolar plate sample are analyzed as one cycle to expose the deformation characteristics of the rubber-pad forming process. There are two different deformation styles for the rubber-pad forming process: one is con-

* Corresponding author at: School of Automotive Engineering, Wuhan University of Technology, Luoshi Load 122#, Wuhan 430070, China. Tel.: +86 27 87168391; fax: +86 27 87168391.
E-mail addresses: liuyx716@163.com, hualin@whut.edu.cn (L. Hua).

0378-7753/$ – see front matter.
doi:10.1016/j.jpowsour.2010.06.078

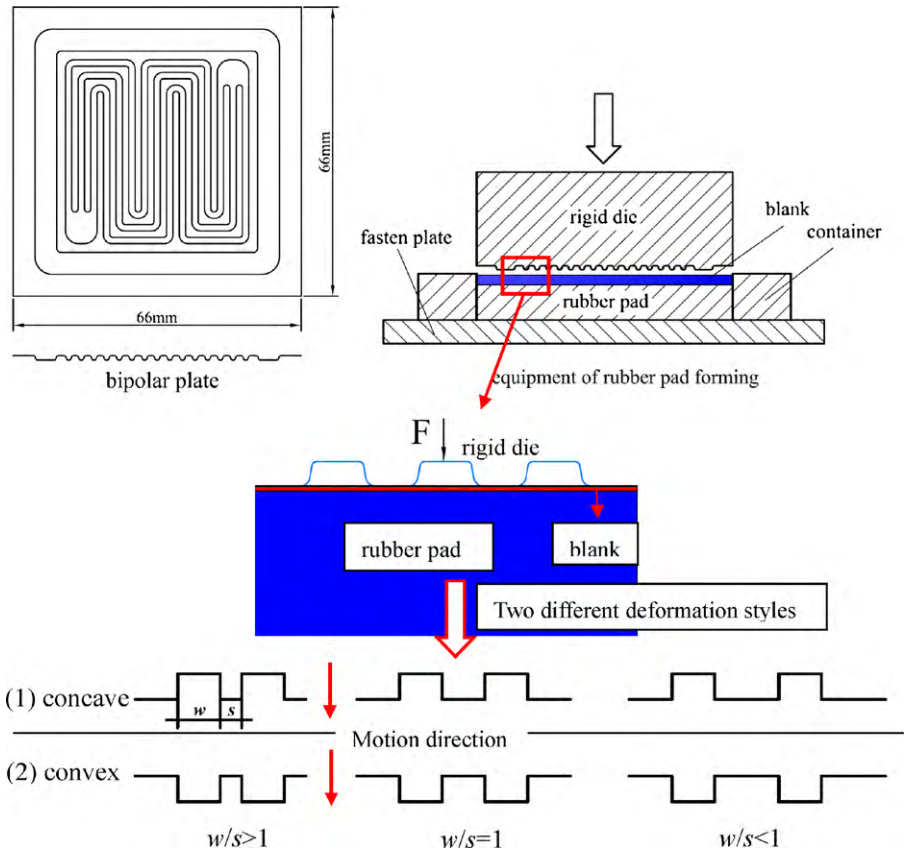

Fig. 1. Fabrication of the bipolar plate by rubber pad forming.

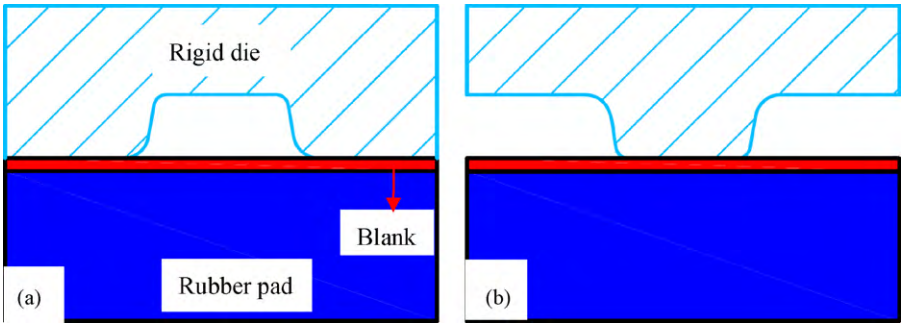

Fig. 2. Sketch of rubber pad forming: (a) concave deformation style and (b) convex deformation style.

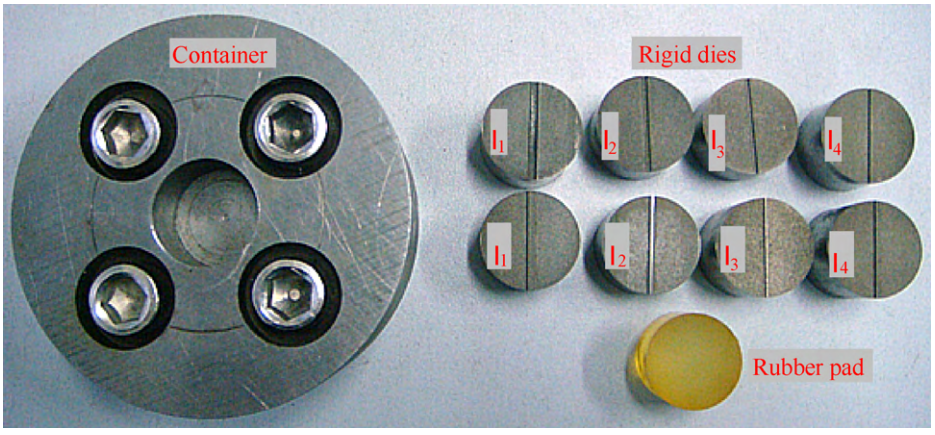

Fig. 3. Photograph of the forming equipment for the experiment.

Table 1
Dimensions of the rigid dies

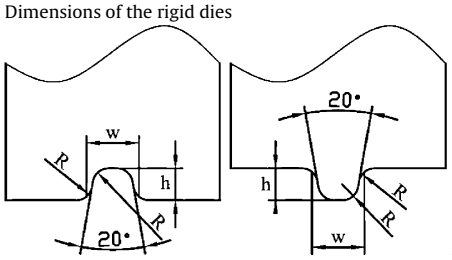

Feature	Depth (h)	Width (w)	Aspect ratio (h/w)	Fillet radius (R)
Dimensions of each channel [mm]				
$I_1/I_2/I_3/I_4$	0.6	2/1.2/0.8/0.6	0.3/0.5/0.7/1	0.3
$II_1/II_2/II_3/II_4$	0.6	2/1.2/0.8/0.6	0.3/0.5/0.7/1	0.3

cave deformation and the other is convex deformation (shown in Fig. 1). However, the characteristics of the two deformation styles have not been studied previously. To obtain high quality products, the rubber-pad deformation style employed to manufacture a certain bipolar plate should be properly selected when the ratio of the channel width w to the rib width s is different ($w/s > 1$, $w/s = 1$, $w/s < 1$). In this paper, the deformation characteristics of single channel forming are analyzed with different deformation styles (Fig. 2). Once these deformation characteristics were obtained, it was easier to determine the proper application conditions for the two styles used to fabricate metallic bipolar plates.

In this study, finite element (FE) simulation and experiment methods are employed to investigate the concave and convex rubber-pad forming process. The forming loads, thickness variation of the formed plates, and effect law of the aspect ratio h/w on the parts formation for the two deformation styles are explored in this paper.

2. Experiments

To investigate the deformation characteristics of the concave and convex rubber-pad forming styles, experiments are conducted and an experimental setup is prepared as shown in Fig. 3. The experimental assembly is composed of three parts: the rubber pad, the container, and the rigid dies. The rigid dies can be divided into two different groups according to the deformation style. The key dimensions of the rigid dies are shown in Table 1. The outer fillet radius and the inner fillet radius are both set as 0.3 mm. To investigate the effect of the channel width w on the forming process, the aspect ratios h/w of the rigid dies range from 0.3 to 1. The channel depth h is held constant at 0.6 mm, and all channels have a 10° draft angle. The rigid dies are manufactured by wire EDM. To maintain the dimensional accuracy, their surfaces are not polished.

The experiments are carried out using a hydraulic press with a capability of 1000 kN. The motion of the working table is controlled by a control panel, and a computer is used to collect the experiment data. Polyurethane rubber with a Shore A hardness of 70 (HD 70) is used as a pad, and a SS304 annealed stainless steel sheet with a thickness of 0.1 mm is used as a blank.

Fig. 4 shows the parts that were manufactured with the velocity of the hydraulic press $v = 0.2\,\mathrm{mm\,s^{-1}}$ and the amount of displacement varied with the rigid die. All the parts successfully achieved the target geometry except I_3 and I_4, which have some micro-cracks on the channel surfaces. While, the investigation of the deformation characteristics of the rubber-pad forming process is a very complicated problem because it involves coupling the deformation between the blank and the rubber during the forming process. Therefore, to analyze the forming process of the two different

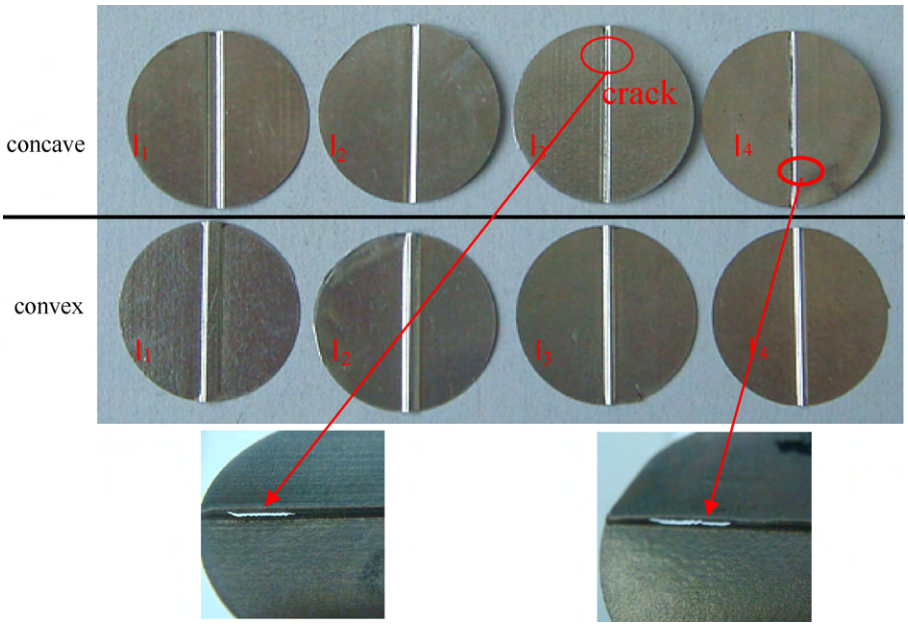

Fig. 4. Parts formed by the concave and convex rubber-pad forming processes.

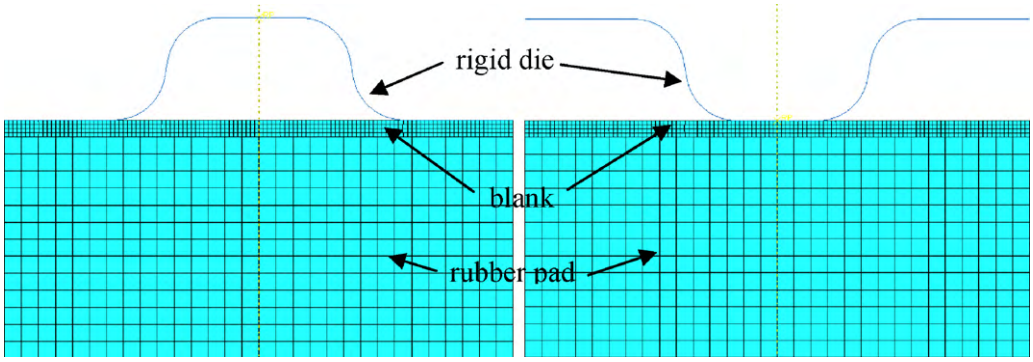

Fig. 5. 2D FE models of the two different deformation styles.

rubber-pad forming styles, a detailed FE simulation is a primary tool used in this study.

3. Numerical simulation

3.1. Finite element (FE) model

Abaqus/Standard, an implicit FE code, is applied to the FE simulations in this study. Because the formed part (Fig. 4) is axial symmetric, to simplify the FE model, one cross-section of the formed part is analyzed and a 2D FE model is created as shown in Fig. 5. The FE model only includes three parts: a rigid die, a blank, and a rubber pad. To simplify the simulation model, the added constraints on the rubber pad due to the container are not considered. The dimensions of the rigid dies are the same as those of the dies used in the experiments (Table 1).

In this model, the punch is modeled as analytically rigid and is not required to be meshed. Four-node bilinear quadrilateral plane strain with reduced integration and hourglass control elements (CPE4R) are applied to model the stainless steel blank. To improve the accuracy of the model, there are four elements in the thickness direction of the blank. Four-node bilinear plane strain quadrilateral hybrid elements with reduced integration and hourglass control (CPE4RH) are employed to describe the rubber pad. These elements are selected based on the following considerations [13]:

1. The blank is modeled as a solid body not as a shell body; therefore, the shell elements are not proper and four-node bilinear quadrilateral plane strain elements are applied.
2. Linear reduced integration elements are insensitive to the distortion of the mesh and have a better property for withstanding serious mesh distortion than full integration elements.
3. Because the elements are inclined to the zero energy deformation mode, called the hourglassing mode, the hourglass control should be considered.
4. When the material is incompressible (Poisson's ratio $\lambda > 0.5$) or is nearly incompressible ($\lambda > 0.475$), such as the case for a rubber-like material, hybrid elements should be applied.

During the rubber-pad forming process, accurately modeling the rubber material is very important because the final geometry of the part depends highly on the deformation of the rubber pad. Generally speaking, the rubber-like material is described as non-linear and hyper-elastic and complies with the incompressible material law, and the Mooney–Rivlin model is usually used to describe its behavior [10]. In this study, a two-parameter (C_{10} and C_{01}) Mooney–Rivlin model is used to describe the polyurethane rubber pad material behavior. Polyurethane rubber with Shore A hardness of 70 (HD 70) is used as the rubber pad in this model. For this rubber material model, the two parameters C_{10} and C_{01} are 0.736 and 0.184 MPa, respectively [10].

An SS304 annealed stainless steel sheet with a thickness of 0.1 mm is used as the blank. The material property of the SS304 is determined by the stress–strain curve obtained from the tensile test [12]. For this material, the elasticity module (E) and Poisson's ratios (ν) are 162.5 GPa and 0.3, respectively. The constitutive relation of annealed SS304 in the tensile plastic deformation can be expressed by Eq. (1):

$$\sigma = (799.9\varepsilon^{0.232} + 60.9)\,\text{MPa} \quad (1)$$

where σ and ε are the true stress and true strain, respectively.

The frictional behaviors between the two different contact pairs (rubber pad-blank; blank-rigid die) are all assumed to follow Coulomb's model [10]. The friction coefficients at the former and later contact pair are considered as 0.2 and 0.1 for lubricated condition, respectively.

As previously mentioned, the container is not created in this model. Therefore, in order to fix the rubber pad correctly, the lower surface of the rubber is held fixed in all directions. The side surfaces of the rubber are fixed in x-direction and are free in y-direction. The rigid die is only allowed to move in the y-direction. The translation of the rigid die can be controlled by velocity the v or a concentrate force F in this model. The velocity v is 0.2 mm s^{-1}.

Moreover, to predict the cracking of the parts in the forming process, the maximum strain theory (a strain-based failure theory) is applied in this model. The input data for the strain-based theory are tensile and compressive strain limits X_t'' and X_c'' in the 1-direction, tensile and compressive strain limits Y_t'' and Y_c'' in the 2-direction,

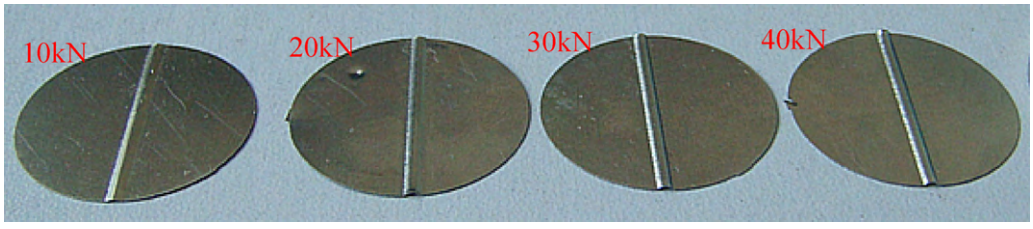

Fig. 6. Parts formed with different forming loads.

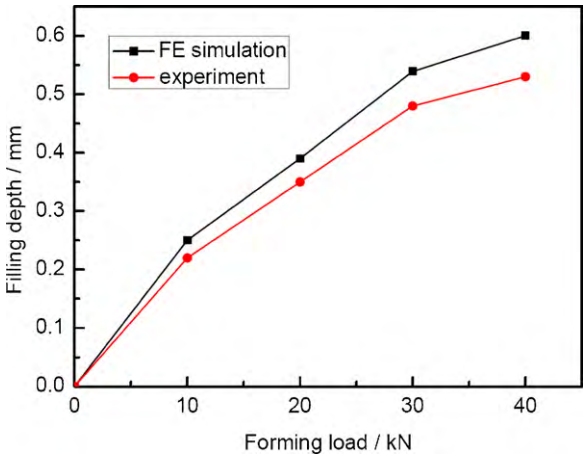

Fig. 7. Comparison of the filling depths of the formed parts between experiment and FE simulation.

and shear strain limit S'' in the X–Y plane. The maximum strain failure criterion requires that the following equation be met:

$$\mathrm{IF} = \max\left(\frac{\varepsilon_{11}}{X''}; \frac{\varepsilon_{22}}{Y''}; \frac{\varepsilon_{12}}{S''}\right) < 1:0 \quad (2)$$

where if $\varepsilon_{11} > 0$, $X'' = X_t''$, otherwise, $X'' = X_c''$; if $\varepsilon_{22} > 0$, $Y'' = Y_t''$, otherwise, $Y'' = Y_c''$.

3.2. Validity of FE analysis

The accuracy of the FE model is very important for the numerical simulation. To verify the accuracy of the FE analysis, the parts (aspect ratio $h/w = 0.5$) are manufactured with different forming loads from 10 to 40 kN. The filling depth of the channel increases with increasing forming load (shown in Fig. 6). Their values are measured and compared with the FE simulation results accordingly, as shown in Fig. 7. It can be seen from this figure that the simulation results are in good agreement with the experimental ones; however, a small difference is observed. The filling depths of the parts in the experiment are smaller than those in the FE simulation. This is because there is a small gap between the rigid die and the container, and the rubber pad will flow into the gap under a high pressure. However, the maximum relative error is only 11.6%, which is acceptable for the numerical simulation. Thus, this 2D FE model of rubber pad forming has proven to be reliable experimentally, and further investigation can be done using the developed 2D FE model.

4. Result and discussion

4.1. Forming process

Peng et al. [7] have studied the concave rubber-pad forming process ($h/w = 0.5$). According to the published research, this forming process contains three different stages (shown in Fig. 8a): the first is the rubber self-deformation; the second is the blank's deformation under the pressure of rubber pad to reach the bottom of rigid die (this process can be called a drawing process); the last stage is the filling of the blank until it fits the rigid die. (This process can be called a bulging process.)

Fig. 8b shows the forming process of the convex deformation style ($h/w = 0.5$). From this figure, the forming process can also be divided into three different stages: the first is the self-deformation of the rubber pad, which is similar to the concave deformation style; the second is the blank blending under the pressure of the rubber pad to reach the side of the rigid die; the last stage is the bulging

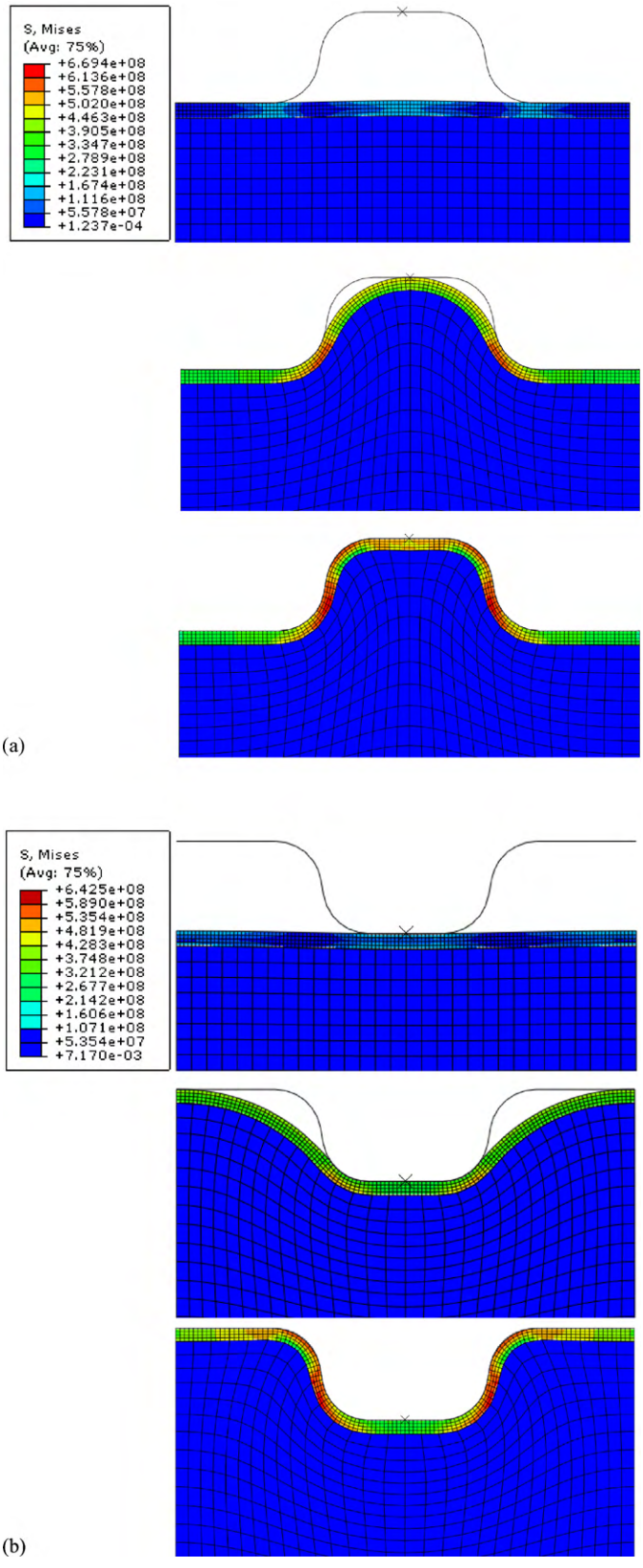

Fig. 8. Forming processes of the rubber pad forming: (a) concave deformation style and (b) convex deformation style ($h/w = 0.5$).

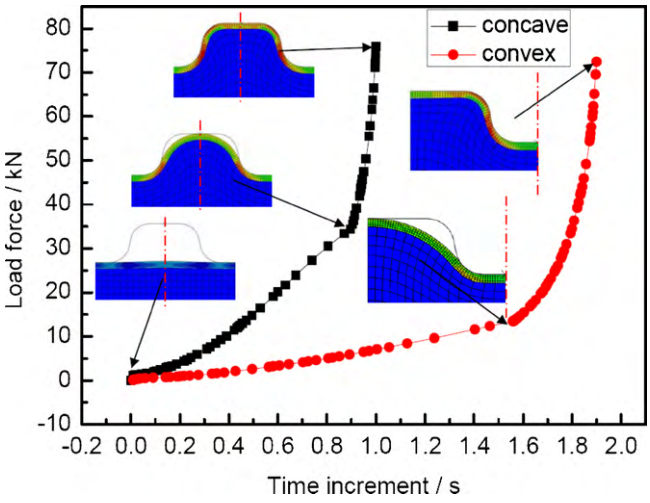

Fig. 9. Forming loads of the two different deformation styles ($h/w = 0.5$).

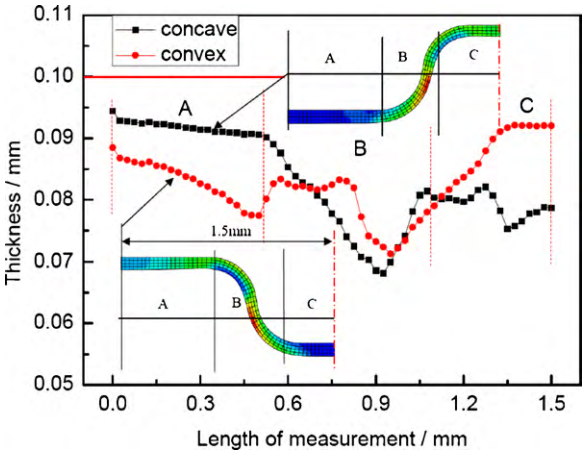

Fig. 10. Thickness variation of the formed parts ($h/w = 0.5$).

process until the blank clings to the rigid die completely. By comparing the two forming processes, the main differences between the concave and convex deformation styles lie in the second forming stage. For the concave deformation style, the second stage is the drawing process, whereas it is the blending process for the convex style.

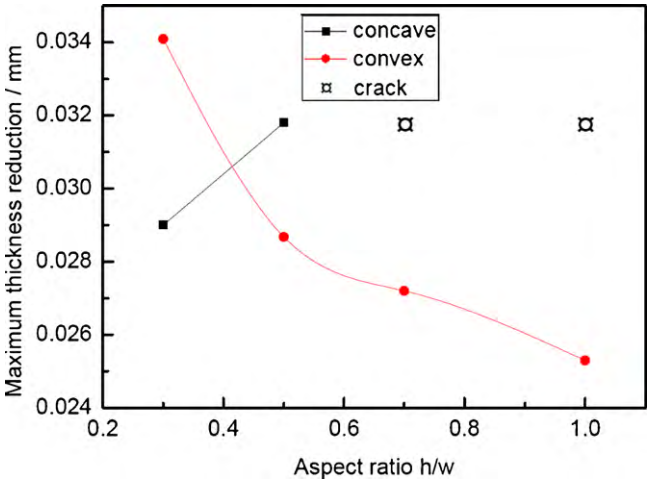

Fig. 11. Maximum thickness reduction of the formed parts with different h/w.

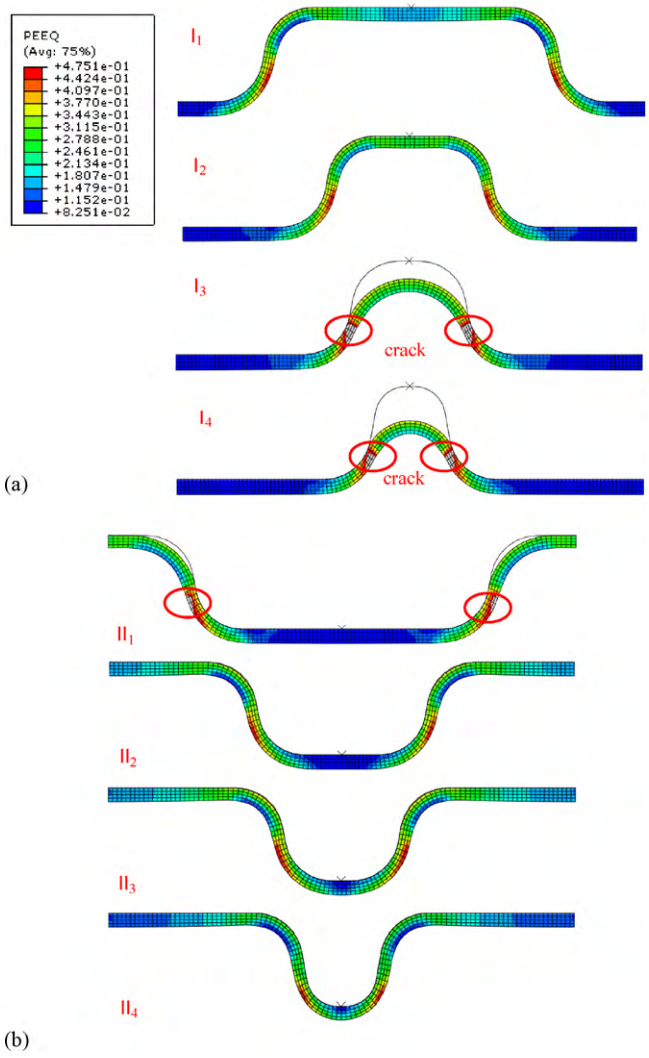

Fig. 12. Formed parts predicted in the FE simulation: (a) concave deformation style and (b) convex deformation style.

4.2. Forming load

Fig. 9 presents the forming load of the two different deformation styles with the velocity of the rigid die $v = 0.2\,\mathrm{mm\,s^{-1}}$ ($h/w = 0.5$). Both forming loads can be divided into three stages corresponding

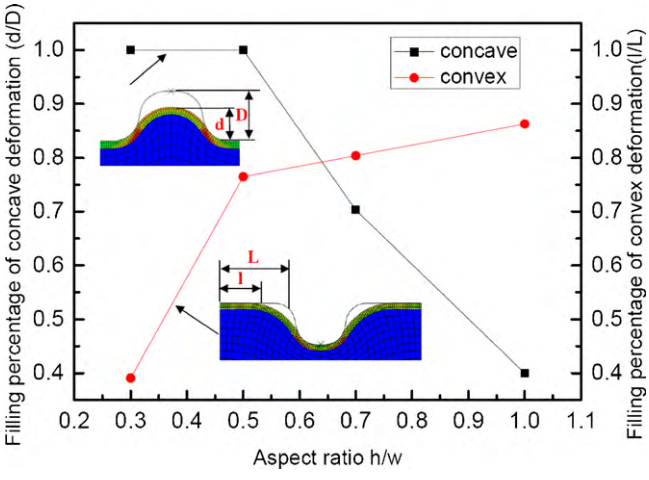

Fig. 13. Effect of h/w on the filling percentage.

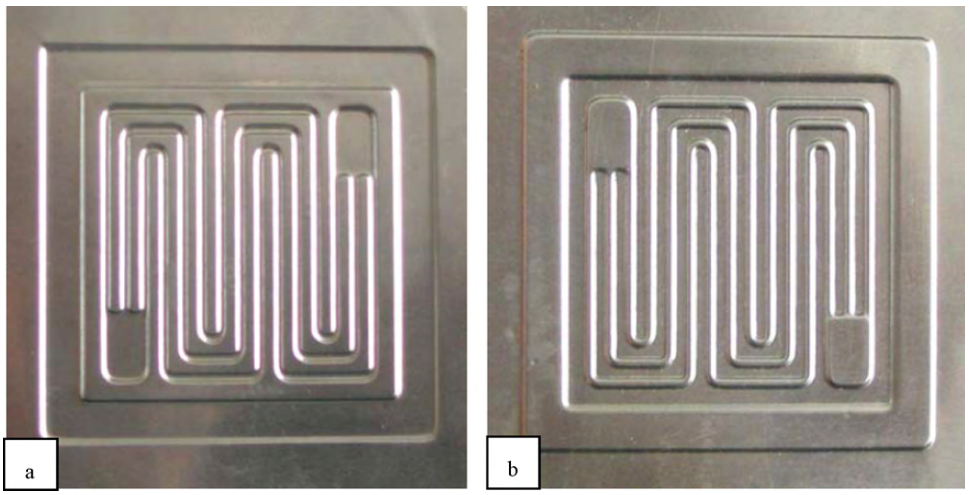

Fig. 14. Sample of a metal bipolar plate fabricated by rubber pad forming: (a) front of the bipolar plate and (b) back of the bipolar plate.

to the forming processes. At the first stage, the rigid die contacts the rubber pad slightly, and the forming load is very small. Then the deformation comes to the second stage, the blank is drawn or blended by the rubber pad, and forming load increases slightly with the increase of time. At the last bulging stage, the blank fills the cavity of the rigid die, and the forming load increases sharply. From Fig. 11, it is also known that the forming load of the concave deformation style increases more sharply than that of the convex style whether at the second stage or the last stage, and the peak forming load is larger than that of the convex deformation style.

4.3. Thickness variation

During the rubber-pad forming process, the thickness of the blank will decrease. To analyze the thickness distribution, the thicknesses of the formed parts are measured. Because the parts are symmetrical, one half-channel of the formed part ($h/w = 0.5$) with a length of 1.5 mm is analyzed as shown in Fig. 10. The curves of the thickness variation with the measured distance can both be divided into three regions. For the concave deformation style, the thickness reduction is very small in region A, which means that the blank in this region deforms slightly. In region B (the side of the channel) and region C (the bottom of the channel) the thickness of the blank decreases rapidly because the drawing process occurs in these two regions. The thinnest point of the part is located in region B, and the thickness reduction of the blank is about 31.8%. Nevertheless, for the convex deformation style, the thickness reduction is very small in region C, and the thickness reduction mainly lies in regions A and B. The thinnest point of the part is also in region B, and the thickness reduction of the blank is about 28.6%, which is smaller than that of the concave deformation style.

Based on the above analyses, the no-deformation area for the concave deformation style is in region A, while for the convex one it is in region C. Moreover, the thickness distribution of the parts manufactured by the convex deformation style is more uniform than that of the concave style when the aspect ratio h/w is equal to 0.5.

To investigate the effect of h/w on the thickness variation, the maximum thickness reductions of the parts formed with different h/w are calculated and summarized in Fig. 11. During the thin sheet metal stamping process, if the maximum thickness reduction reaches a critical value, the parts will be cracked, and this phenomenon should be avoided in real applications. Fig. 11 shows that, for the convex deformation style, as the value of h/w increases, the maximum thickness reduction decreases. Contrarily, for the concave style, the maximum thickness reduction increases with increasing h/w, and the parts are even cracked for $h/w = 0.7$ or $h/w = 1$.

4.4. Effect of h/w on the forming process

Fig. 12 shows the formed parts predicted in the FE simulation. The aspect ratios applied in the simulation are the same as those in the experiment (Table 1). For the concave deformation style, I_1 and I_2 fill the cavity of the rigid die perfectly, but I_3 and I_4 will be cracked during the forming process. However, for the convex style, all the parts have been formed well except II_1, which is at risk of cracking. Therefore, the effect of the channel width on the part formation is different for the two deformation styles.

To compare the difficulty level of parts formation of the two deformation styles, these parts are formed with a forming load $F = 50$ kN. For the concave deformation style, the ratio of filling depth to the depth of cavity of the rigid die (d/D) is applied to define the filling percentage, and l/L is applied for the convex deformation style (shown in Fig. 13). According to Fig. 13, under the same action of forming load, a larger h/w makes it more difficult to fill the cavity of the rigid die using the concave deformation style and makes it easier to fill the cavity using the convex style.

4.5. Discussion

Based on the above analysis, for the concave deformation style, as the channel width decreases, it is more difficult to fill the cavity of the rigid die, and the thickness reduction of the formed parts is increased. On the contrary, for the convex deformation style, as the channel width decreases, the formation of the parts becomes easier, and the thickness reduction of the formed parts becomes smaller. Therefore, for the fabrication of a high quality metallic bipolar plate (shown in Fig. 1), if the ratio of the channel width to the channel rib $w/s > 1$, the concave deformation style of rubber-pad forming process is more appropriate, otherwise, the convex style is preferred.

According to the bipolar plate sample we designed [12], the flow channel depth h is 0.5 mm, the flow channel width w is 0.8 mm, and the rib width s is 1.2 mm. Therefore, the aspect ratio $h/w = 0.66$, and the ratio of the channel width to the rib width $w/s < 1$. This plate is therefore suitable to be fabricated by adopting the convex deformation style. Fig. 14 shows the metallic bipolar plate (SS304, with a thickness 0.1 mm) manufactured by the convex rubber-pad

forming process. The plate has a high surface quality and is not cracked or winkled.

5. Conclusion

In this study, the deformation characteristics of the concave and convex rubber-pad forming processes are analyzed in detail with numerical simulation and experimental methods. Based on the FE simulation, the proper condition for the two deformation styles is determined. From this study, we arrive at the following conclusions:

(1) The forming processes of the two deformation styles can be divided into three stages, and the second stages are different for the two styles. When the aspect ratio $h/w = 0.5$, the forming load is larger for the concave deformation style, but the thickness distribution of the plate fabricated by this deformation style is more uniform that that of the concave style.
(2) For the convex deformation style, as the value of h/w increases, the maximum thickness reduction decreases. Contrarily, for the concave style, the maximum thickness reduction increases with increasing h/w.
(3) The ratio of the channel width to the rib width determines which deformation style is suitable for the bipolar plate fabrication. When $w/s > 1$, the concave style is more appropriate; otherwise, the convex one is preferred. A bipolar plate sample ($w/s < 1$) is manufactured by the convex rubber-pad forming process.

Acknowledgment

The authors would like to thank the Natural Science Foundation of China for Distinguished Young Scholars (No. 50725517).

References

[1] J.W. Lee, H.C. Kwon, M.H. Rheec, Y.T. Im, J. Mater. Process. Technol. 140 (2003) 487–493.
[2] M.W. Fu, S.Q. Lu, M.H. Huang, J. Mater. Process. Technol. 52 (1995) 359–367.
[3] H.A. Al-Qureshi, J. Mater. Process. Technol. 125–126 (2002) 751–755.
[4] C. Hindman, K.B. Ousterhout, J. Mater. Process. Technol. 99 (2000) 38–48.
[5] M.W. Fu, H. Li, J. Lu, S.Q. Lu, Comput. Mater. Sci. 46 (2009) 1058–1068.
[6] X.M. Jiang, M. Tian, J.Y. Zhang, The Application of the Polyurethane Rubber in the Field of Stamping Technology, Defense Industry, Academic Press, Beijing, 1989.
[7] L.F. Peng, P. Hu, X.M. Lai, D.Q. Mei, J. Ni, Mater. Des. 30 (2009) 783–790.
[8] D.J. Browne, E. Battikha, J. Mater. Process. Technol. 55 (1995) 218–223.
[9] G. Salau, Mater. Des. 22 (2001) 299–315.
[10] M.H. Dirikolu, E. Akdemir, J. Mater. Process. Technol. 148 (2004) 376–381.
[11] M. Ramezani, Z.M. Ripin, R. Ahmad, J. Mater. Process. Technol. 209 (2009) 4925–4934.
[12] Y.X. Liu, L. Hua, J. Power Sources 195 (2010) 3529–3535.
[13] Abaqus Theory Manual, Version 6.3. Hibbitt, Karlsson and Sorensen Inc., Pawtucket, RI, USA, 2002.